Suppression of Lateral Phase Separation in Thin Polyolefin Blend Films

Y. A. Akpalu*,† and A. Karim*

Polymers Division, National Institute of Standards and Technology, Gaithersburg, Maryland 20899-8542

S. K. Satija

NIST Center for Neutron Research, National Institute of Standards and Technology, Gaithersburg, Maryland 20899-8542

N. P. Balsara

Department of Chemical Engineering, Six Metrotech Center, Polytechnic University, Brooklyn, New York 11201

Received August 1, 2000; Revised Manuscript Received December 19, 2000

ABSTRACT: The effectiveness of a compatibilizer in suppressing lateral phase separation in thin polyolefin blend films is investigated as a function of film thickness and temperature. Neutron and X-ray reflectivity measurements were made on spun-cast thin blend films of partially deuterated and hydrogenated polyolefin blends with and without diblock compatibilizer. We use an extended silicon surface passivating treatment. Under these biased symmetric wetting conditions (air vs hydrophobic Si), binary blend films are stabilized against both dewetting from the substrate and roughening of the surface due to phase separation when the film thickness (≈25 nm) is on the order of the molecular radius of gyration. However, thicker (≈100 nm) films exhibit lateral phase separation that can be suppressed by the addition of block copolymer compatibilizer. This stabilization effect can be attributed to the reduction of interfacial tension leading to a broadening of interfaces, and additionally, the presence of diblock copolymer in both phases alters their surface interactions. On longer time scales, optical micrographs show the development of large-scale features over the course of a year in the molecularly thin blend films and in the ternary thin film (stored under vacuum). A droplet morphology is observed for molecularly thin blend films, and an interconnected domain structure characteristic of the early and intermediate stages of phase separation is observed for the ternary thin blend film. The phase separated structure obtained for the binary thin blend film does not evolve with time. Our results indicate that one also needs to account for kinetics in order to develop a comprehensive understanding of the structure of thin blend films. In general, temperature has a weak effect on the profile development of compatibilized blend films.

Introduction

The enhanced stability of thin polymer films (<100 nm) on solid substrates has important technological and scientific ramifications. Interest in thin films range from applications such as optics and microelectronics, contact lenses, paints, and multilayer packages for food to fundamental studies of polymer diffusion and adsorption.[1,2] The production of stable defect-free films is particularly problematic in thin films where the unstable growth of capillary waves driven by dispersion forces across an initially uniform film tend to cause film rupture.[3−11] However, paints, adhesives, and lubricants are typically multicomponent polymer systems. Therefore, it is important to investigate the stability and structure of multicomponent thin film polymer blends.

The behavior of phase-separated polymer blends in the bulk after quenching into the unstable region of the phase diagram has been studied[12−15] intensively. In the bulk, the concentration fluctuations that govern the phase separation process are random. As a result, the final morphology consists of mutually interconnected domain structures rich in a given blend component that coarsen slowly with time. In thin films where the thickness of the sample is much smaller than its lateral extensions, surface effects cannot be neglected and the spatial isotropy of the phase separation process is broken. The presence of additional interfaces (polymer/surface and polymer/substrate) causes the directions of the compositional waves in the polymer mixture close to the interfaces to be modified such that phase separation occurs laterally in the plane of the film.[16−23] While the air surface prefers the lower surface energy phase, the substrate interfacial preference can change from one blend component to another if the nature of the substrate surface is altered.[17−20,24] Hence, the phase morphology and its time evolution in thin, phase-separated polymer films are governed by the interplay between phase-separation processes and the interactions of the polymer phases with the air and the substrate.

In thin polymer blend films where the film thickness (D) is much larger than the bulk correlation length, spatially decaying composition waves with a characteristic length, $h(t)$, are induced by the presence of a surface and grow normal to the surface during phase separation.[18] The growth law of $h(t)$ is governed by the same dynamical scaling relations as in the bulk.[25] For many polymers the characteristic length scale during the initial stages of phase separation, namely the spinodal wavelength l_{sp}, is on the order of $l_{sp} \sim O(100\ \text{nm})$.

† Current address: New York State Center for Polymer Synthesis, Department of Chemistry, Rensselaer Polytechnic Institute, Troy, NY 12180. E-mail: akpaly@rpi.edu.

* To whom correspondence should be sent.

10.1021/ma001347p CCC: $20.00
Published on Web 02/10/2001

Table 1. Molecular Characterization of Polymers[13,14,46]

sample	$10^{-4}M_w$	M_w/M_n	ρ (g/cm^3)	n_D	N	l (Å)[a]	R_g (Å)
hPM	17.3	1.07	0.8540		2500	8.19	167
dPE	23.8	1.08	0.9226	6.15	2600	7.93	165
HPE−hPM	4.6	1.09	0.8579		300−300	7.93−8.19	114

[a] Reference volume for l (Å) is 148.6 (Å^3).[14]

If the film thickness is reduced to a scale (L_c) on the order of l_{sp}, the "surface-directed" spinodal waves from both surfaces of the substrate interfere.[20] The interference can be constructive or destructive depending on film thickness, as observed in both experiments and computer simulations. If the film thickness is comparable to or smaller than l_{sp} but much larger than the molecular radius of gyration (R_g), "surface-directed" spinodal decomposition is suppressed.[21] Transient surface roughening in films somewhat thicker than L_c was attributed to hydrodynamic flows and dewetting.[26] Recent studies[21−23] on films ($D = L_c$) have attributed nontransient surface roughening to the lateral phase separation within the film and associated variations of surface tension within the film that cause the film to buckle. This implies that the surface roughening has a thermodynamic origin. The surface structure essentially "mirrors" the composition variations within the film. The observations of a bicontinuous spinodal decomposition pattern in near critical symmetric binary blend films and a dropletlike or holelike surface morphology in off-critical blends by Ermi et al.[22] are consistent with the expected underlying domain structure at these compositions. Moreover, Ermi et al.[22] confirm the thermodynamic nature of the surface roughening by observing the homogenization of the surface structures at both compositions when the film is returned into the single-phase region through a change in temperature. Notably, this homogenization process was only possible when the phase separation had not proceeded to late stages.

In contrast to these earlier measurements, we focus on the effect of a compatibilizing copolymer on film stability and phase separation induced surface roughening in very thin films where D is on the order of the radius of gyration (R_g) of the chains ($1 < D/R_g < 5$). As one decreases the film thickness there comes a point where there is not enough material in the interior of the film to sustain lateral phase separation due to the distribution of material in the form of boundary wetting layers. Moreover, the factors that govern the long- and short-term stability of polymer films in this thickness range are not well understood experimentally. Recent computer simulations[27,28] for films in this thickness range have been reported, but these simulations have not been validated by measurements. It is then unclear what form phase separation should take in such thin films.

The addition of copolymers (e.g., block,[29−34] comb,[35] and random)[36] to binary mixtures usually alters the critical temperature and critical composition for phase separation. In practice, these shifts can be large, leading to both increase and decrease of the phase stability of the mixture.[37−42] The phase separation of polymer blend films (≈200 nm) containing a relatively high concentration (30%) of diblock copolymer has been recently reported.[43] Interestingly, the addition of a diblock to the binary mixture resulted in a bicontinuous pattern that did not evolve appreciably over relatively long time scales (days to weeks). In the bulk, the diblock copolymer of this study forms spherical micelles. The substantial reduction in size of the phase-separated domains and the stabilization of the bicontinuous structure observed were attributed to the "entropic" inhibition of phase separation into micelles, owing to confinement. In a separate study,[44] the addition of a block copolymer to a polymer film caused a suppression of the roughening of the film due to phase separation.

With regard to the blends we study in the present paper, the addition of a diblock copolymer to the binary mixture has been shown to increase the phase stability for bulk films (thickness $D \approx$ mm).[14] For the copolymer concentrations of interest in our study, quantitative evidence for the absence of concentrations fluctuations that may lead to the formation of large aggregates of copolymer chains such as micelles was obtained from small-angle neutron scattering measurements.[13,14]

In this paper, we investigate the effect of a compatibilizing copolymer (whose molecular mass is much smaller than the homopolymer blend components) on film stability and phase separation induced surface roughening phenomena as a function of film thickness and temperature. We use an extended silicon surface passivating treatment that makes the silicon surface strongly hydrophobic.[45] Under these biased, but qualitatively symmetric wetting conditions, binary blend films are stabilized against both dewetting from the substrate and surface roughening when the film thickness (≈25 nm) is on the order of the radius of gyration. However, thicker (≈100 nm) films exhibit lateral phase separation that is suppressed by the addition of a block copolymer compatibilizer. The short-term stabilization is due to a complex interplay of surface enrichment of one blend component, film thickness, and the distribution of block copolymer in the film.

Experimental Section

We perform measurements on partially deuterated poly(ethylbutylene) (dPE), poly(methylbutylene) (hPM), and block copolymer poly(ethylbutylene)-*block*-poly(methylbutylene) (hPE−hPM). Table 1 summarizes the characteristics[13,14,46] of the polymers used in this work. The symmetric dPE/hPM blend exhibits an upper critical solution temperature ($T_{UCST} \approx 130$ °C) while the UCST of the hPM/dPE/hPM−hPE ($\phi_{hPE-hPM} = 0.2$, $\phi_{dPE} = 0.4$) is about 80 °C.[14]

Blend films were spun cast from toluene solutions onto hydrophobic, silicon (Si) wafers. Prior to spin coating, the wafers were acid cleaned in a bath of 70/30 volume ratio solution of 96 H_2SO_4 30% H_2O_2 for 1.5 h at 80 °C, etched using a buffered oxide etch solution and passified with a 40% aqueous ammonium fluoride solution, rinsed thoroughly with deionized water, and dried under N_2. All chemicals used for etching were purchased from J.T. Baker.[47] For blend films that were spun cast onto wafers cleaned by the procedure described, X-ray reflectivity measurements show that the resulting as-cast films are stable under vacuum at room temperature for several days. The film thickness could be controlled by varying the solution concentration at a fixed spin speed; e.g., a toluene solution with a dPE/hPM total polymer mass fraction of 0.44% spun at 1000 revolutions per minute (rpm) produced a blend film with a thickness of 22 nm. The thicknesses of all films prepared were determined by X-ray reflectivity measurements, and the results are shown in Table 2. An optical microscope

Table 2. Calculated Coherent Scattering Length Densities, *B/v*, of Materials Using Tabulated Literature Values[1]

material	$10^4 b/v$ (nm^{-2})	material	$10^4 b/v$ (nm^{-2})
air/vacuum	0	hPM	−0.302
Si	2.09	dPE	3.6
SiO_2	3.48	HPE−hPM	−0.303

(Nikon Optiphot-2)[47] coupled to a CCD camera (Kodak model ES 1.0)[47] was also used to characterize the morphology before and after annealing. Optical microscopy indicated that the as-cast blend films were smooth and uniform when inspected immediately after spin coating.

Neutron reflectivity measurements were conducted on the NG-7 reflectometer at the NIST Center for Neutron Research (NCNR). At NG-7, neutrons of fixed wavelength (4.76 Å) were collimated and reflected from the horizontally placed sample. The reflected beam is detected by a shielded He^3 pencil detector at a reflection angle that is the same as the angle of incidence, and the incident, reflected, and film normal are in one plane (specular reflectivity). The desired neutron momentum (q) range was attained by changing the angle of incidence (θ) while keeping the detector at an angular position of 2θ with respect to the incident beam. All measurements were performed in-situ in a vacuum chamber at room temperature and elevated temperatures. Compatibilized blend films of dPE/hPM/hPE−hPM were annealed at 35, 45, 55, and 80 °C while dPE/hPM films were annealed at 50, 74, 99, and above 120 °C. Neutron reflectivity spectra were recorded after annealing samples for 120 min at each temperature. The annealed samples were then characterized by X-ray and reflective optical microscopy within 24 h of quenching the samples to room temperature. The X-ray and neutron reflectivity data were fit by using a standard multilayer fitting routine for scattering length densities.[48,49] The coherent scattering length densities for pure materials are listed in Table 2. In all figures, the standard deviations in the quantities estimated from NR and XRR are plotted only when the uncertainty limits (standard deviation) are larger than the symbol size of plotted points.

Results

The evolution of the phase-separated structure in dPE/hPM and dPE/hPM/hPE−hPM blends in the bulk has been followed by time-resolved neutron scattering and light scattering.[13,14] The objective of these studies was to compare the structural evolution of the phase-separated structures with theoretical predictions based on the random phase approximation and classical signatures of spinodal decomposition. The theoretically predicted stabilization (lowering of the UCST) of the phase boundary due to the compatibilizing effect of the block copolymer was observed. The measured critical temperature (T_c) for a dPE/hPM blend ($\phi_{dPE} = 0.5$) is about 130 °C while that for a ternary blend of dPE/hPM/hPE−hPM with $\phi_{hPE-hPM} = 0.2$ and $\phi_{dPE} = 0.4$ is about 80 °C.[14]

Our present study of the dPE/hPM and dPE/hPM/hPE−hPM blends is aimed at gaining insight into the stability and structure of thin films of these blends in the phase-separated state. We monitored the evolution of spun-cast films of dPE/hPM and dPE/hPM/hPE−hPM by neutron reflectivity after annealing samples at progressively higher temperatures in the bulk two-phase region of the phase diagram, i.e., at temperatures below the spinodal temperature for an upper critical solution temperature (UCST) system. The compositions of the hPM/dPE/hPM−hPE blends are (a) $\phi_{dPE} = 0.5$, $\phi_{hPE-hPM} = 0.0$ and (b) $\phi_{dPE} = 0.4$, $\phi_{hPE-hPM} = 0.2$ where ϕ_i is the volume fraction of component i, i = hPM, dPE, or hPE−hPM, and by assuming incompressibility $\phi_{dPE} + \phi_{hPM} + \phi_{hPE-hPM} = 1$. Hence, the blends are completely described by two concentration variables: ϕ_{dPE} and $\phi_{hPE-hPM}$.

In thin films, the stability of the film morphology is known to depend on thickness. For thin blend films, this can be even more complicated by the phase separation process. Hence, in order to investigate effects arising from the possible compatibilization of the diblock copolymer, we studied each blend at two thicknesses. The thicknesses of the blend films (20−100 nm) used in our studies are much smaller than the measured characteristic length scale ($l_{sp} = 200$ nm)[14] during the initial stages of spinodal decomposition. In the following discussion, B1 and B2 (binary blends) will refer to 84 and 22 nm thick blends with no copolymer. T1 and T2 (ternary polymer mixtures) will refer to 100 and 23 nm thick films with a copolymer volume fraction of 0.2. We define thin films by the condition that the ratio of the thickness D to the molecular radius of gyration (R_g) is larger than 2 and molecularly thin films where $1 < D/R_g < 2$.[28] Hence, B1 and T1 are thin films since $D/R_g \approx 5$, and B2 and T2 are molecularly thin films.

Our approach to studying the stability and structure of our molecularly thin and thin blend films was to characterize the structure of the as-cast films by X-ray reflectivity and optical microscopy to establish the initial state of the films. Neutron reflectivity was then used to probe changes in the internal distribution of deuterated and nondeuterated polymer (averaged in the film plane) as films were progressively annealed at higher temperatures in the bulk two-phase region. Binary blend films B1 and B2 were "fully annealed" following annealing at 50, 74, 99, and 123 °C while ternary blend films T1 and T2 were "fully annealed" after 35, 45, 55, and 80 °C. NR samples were annealed after each temperature change in-situ under vacuum for about 2 h before the NR spectra was recorded. After 2 h no changes are observed, and the total annealing time at each temperature is 4 h. The "fully annealed" films were then characterized by X-ray and optical microscopy after quenching the blend films from the highest annealing temperature to room temperature under vacuum.

Neutron and X-ray reflectivity techniques have been described in detail elsewhere.[1] In any scattering or reflectivity measurement it is necessary to have contrast between the species of interest and the surrounding medium. Because of the different scattering lengths for hydrogen and deuterium, neutron reflectivity can be used to detect variations in the scattering length density (b/v) as a function of depth (z). These variations in the scattering length density can be used to provide information on the structural details in the direction normal to the film plane (z direction). The b/v measured in an NR experiment is the average b/v in the film plane. Neutron scattering length densities for the polymers studied are shown in Table 3.

For X-rays, differences in the electron density give rise to a nonuniform scattering length density profile which in turn results in a characteristic reflectivity profile. Since there is negligible electron density contrast for the hydrogenated (hPM, hPE−hPM) and deuterated (dPE) polymers used in this study, the X-ray reflectivity profiles are only sensitive to the roughnesses at the air/polymer and polymer/silicon interfaces. On the other hand, NR is sensitive to variations in the roughness of the polymer/polymer, air/polymer, and polymer/silicon

Table 3. Film Thickness, Air/Polymer Roughness (σ_{air}), and Polymer/Substrate Roughness (σ_{Si})[a] of DPE/HPM/HPE−hPM Blend Samples Determined from X-ray Reflectivity

symbol	blend composition	thickness (nm)	σ_{air} (Å)	σ^{A}_{air} (Å)	σ_{Si} (Å)	σ^{A}_{Si} (Å)
B1	$\phi_{dPE} = 0.5$; $\phi_{hPE-hPM} = 0.0$	84	8.9	46.0	3.4	5.5
B2	$\phi_{dPE} = 0.5$; $\phi_{hPE-hPM} = 0.0$	22	7.2	8.1	6.0	6.4
T1	$\phi_{dPE} = 0.4$; $\phi_{hPE-hPM} = 0.2$	100	8.9	11.1	1.3	4.3
T2	$\phi_{dPE} = 0.4$; $\phi_{hPE-hPM} = 0.2$	23	6.8	9.4	5.5	6.0

[a] The roughnesses obtained for the annealed samples after quenching are denoted as σ_i^A where i = air or Si. The relative standard deviation in the values shown is less than 1%.

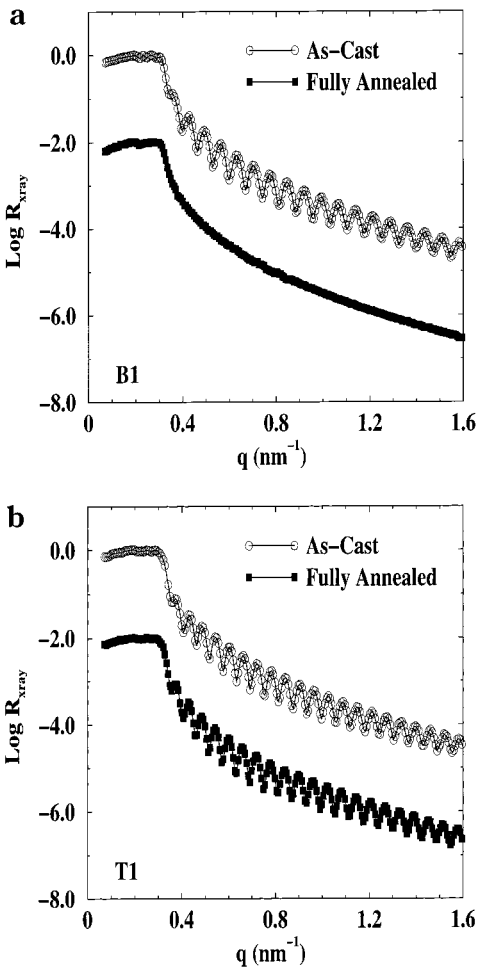

Figure 1. X-ray reflectivity from as-cast and "fully annealed" thin blend films (a) B1 and (b) T1. See text for the definition of "fully annealed".

interfaces. For both NR and XRR, the damping of oscillations as the roughness of the interfaces increase is more pronounced at higher q. The XRR roughnesses at the various interfaces for different samples are summarized in Table 3.

X-ray reflectivity (XRR) data obtained on as-cast and "fully annealed" thin films are shown for B1 (Figure 1a) and T1 (Figure 1b). From XRR, we obtain minor differences in the air/polymer roughness of the as-cast and "fully annealed" samples of B2, T1, and T2 while the air/polymer roughness of "fully annealed" B1 is about 5 times larger than that of as-cast B1 (Table 2). The large air/polymer roughness coupled with the absence of fringes in the XRR profile of "fully annealed" B1 (Figure 1a) strongly suggests the presence of long-wavelength surface features.

Representative neutron reflectivity (NR) data of B1 and T1 films obtained at the different annealing temperatures are shown in Figures 2 and 3, respectively.

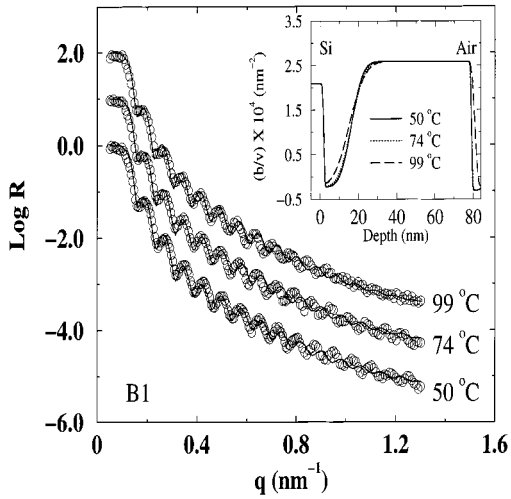

Figure 2. Neutron reflectivity from B1 as a function of neutron momentum transfer, q, perpendicular to the film surface. Open circles denote experimental data, while the solid lines indicate the best-fitted curve calculated from the scattering length density profiles shown in the inset. The NR spectra were obtained after annealing the film for 120 min under vacuum at the temperatures shown.

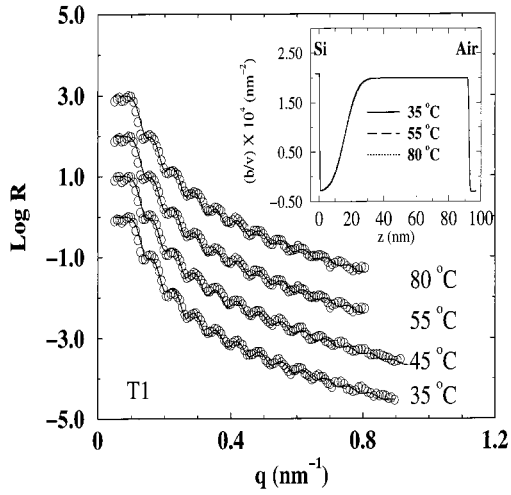

Figure 3. Neutron reflectivity from T1 as a function of neutron momentum transfer, q, perpendicular to the film surface. Open circles denote experimental data, while the solid lines indicate the best-fitted curve calculated from the scattering length density profiles shown in the inset. The NR spectra were obtained after annealing the film for 120 min under vacuum at the temperatures shown.

For both B1 and T1, the b/v profiles shown in the inset demonstrate an enrichment of lower scattering length density hPM over dPE to the air as well as silicon interfaces. In contrast to the large differences in the XRR profiles of as-cast and "fully annealed" B1 films, NR profiles for B1 show a gradual broadening of the polymer−polymer interfaces near the air and silicon

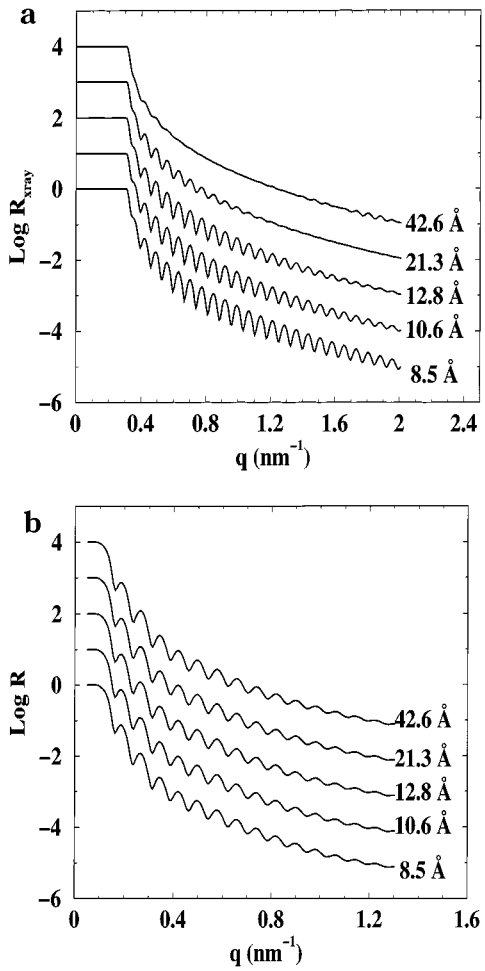

Figure 4. Model reflectivity profiles and corresponding scattering length density profiles for B1 as the air roughness is increased from 8.5 to 42.6 Å: (a) X-ray and (b) neutrons. Calculations were performed by using the fitted values for the silicon−polymer and polymer−polymer roughnesses for the as-cast film.

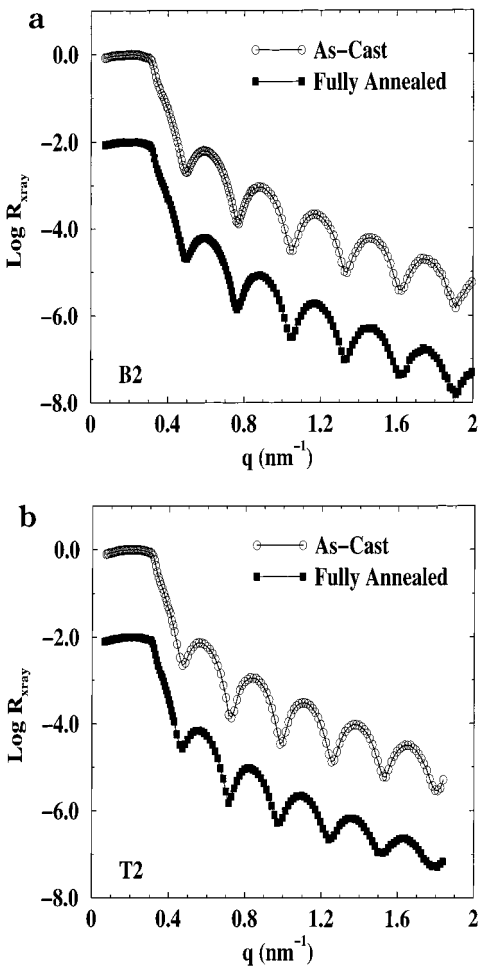

Figure 5. X-ray reflectivity from as-cast and "fully annealed" molecularly thin blend films (a) B2 and (b) T2. See text for the definition of "fully annealed".

boundaries as the annealing temperature is increased (Figure 2).

The development of large-scale surface features in B1 can result from the roughening of the air−hPM rich interface with or without any changes in the polymer−polymer interfaces within the film. To illustrate how the roughening of the air−hPM rich interface will manifest in NR and XRR when the air roughness increases, we calculated model X-ray and neutron reflectivity profiles for as-cast B1 as the roughness of the air−hPM rich interface is varied from 8.5 Å (as-cast air−hPM roughness) to 42.5 Å ("fully annealed" air−hPM roughness). For X-rays, one sees a slight damping of the oscillations as one increases the roughness from 8.5 to 10.6 Å and complete damping by 42.5 Å (Figure 4a). In contrast, very little changes are observed in the neutron reflectivity profiles (Figure 4b). Hence, if we combine the NR and XRR information in B1, the slight broadening of the b/v profile near both boundaries and the increased damping of oscillations in the reflectivity profile at high q ($q > 0.1$) with temperature indicate a continuous increase in the roughening or undulations of the air−film boundary and the polymer−polymer interfaces (Figure 2). In contrast, T1 does not show any changes in the profile near the boundaries that can be detected by neutron reflectivity (Figure 3) or XRR (Figure 1b) in the temperature region (above 74 °C) where damping of oscillations in the neutron reflectivity profile of B1 is observed. For T1, our results indicate that even if surface undulations developed during the annealing of the block copolymer containing blend in the two-phase region, the periodicity of the undulations are much smaller than that obtained for B1. Essentially, these results (B1 and T1) demonstrate the effect of adding the diblock in "thin" films.

To determine the film thickness dependence of the suppression of lateral phase separation for the blend compositions, we investigated the thinner "molecularly thin" films ($L \approx 25$ nm). XRR profiles for as-cast and "fully annealed" B2 and T2 films are shown in Figure 5. For both molecularly thin films, the absence of visible changes in the prominent XRR fringes (Figure 5) (negligible changes in the roughness at the substrate and air interface after annealing) suggests the absence of surface roughening and long-wavelength surface features. Figure 6 shows representative NR data obtained for B2 while NR data for T2 is shown in Figure 7. For B2 and T2, the b/v profiles shown in the inset also demonstrate an enrichment of lower scattering length density hPM over dPE to the air as well as silicon interfaces and show that the profiles are insensitive to temperature.

The effect of a strongly attractive surface on the distribution of hydrogenated and deuterated polymer as a function of depth can be deduced from concentration depth profiles (Figure 8). By assuming incompressibility,

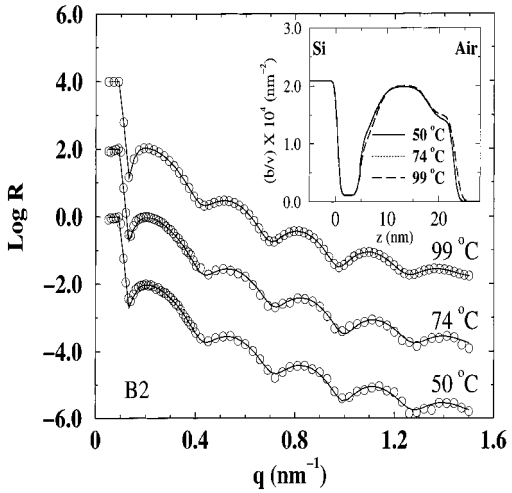

Figure 6. Neutron reflectivity from B2 as a function of neutron momentum transfer, q, perpendicular to the film surface. Open circles denote experimental data, while the solid lines indicate the best-fitted curve calculated from the scattering length density profiles shown in the inset. The NR spectra were obtained after annealing the film for 120 min under vacuum at the temperatures shown.

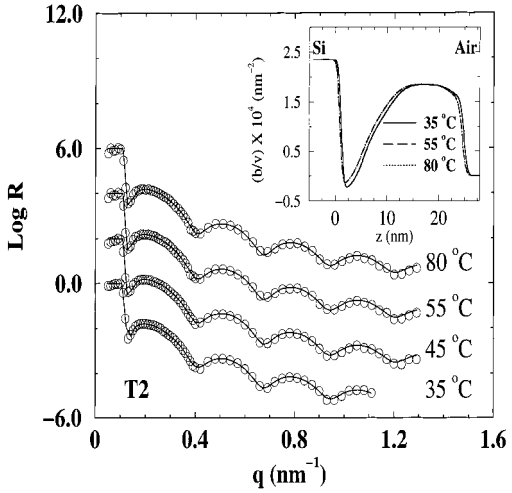

Figure 7. Neutron reflectivity from T2 as a function of neutron momentum transfer, q, perpendicular to the film surface. Open circles denote experimental data, while the solid lines indicate the best-fitted curve calculated from the scattering length density profiles shown in the inset. The NR spectra were obtained after annealing the film for 120 min under vacuum at the temperatures shown.

the relation between the b/v profiles and concentration is

$$(b/v)(z) = \sum_i (b/v)_i(\phi)_i(z) \quad (1)$$

$$\sum_i \phi_i(z) = 1 \quad (2)$$

where $(b/v)_i$ and $\phi_i(z)$ are the b/v value of pure i (see Table 2) and its volume fraction at z along the direction perpendicular to the film surface, respectively. In Figure 8, concentration depth profiles for dPE $\phi_{dPE}(z)$ in B1 and B2 at 50 °C are compared to T1 and T2 at 55 °C. At these temperatures, the pinned layered structure suppresses the coarsening of domains due to lateral phase separation such that no changes in the profiles are observed in a 24 h period. This property allows us to

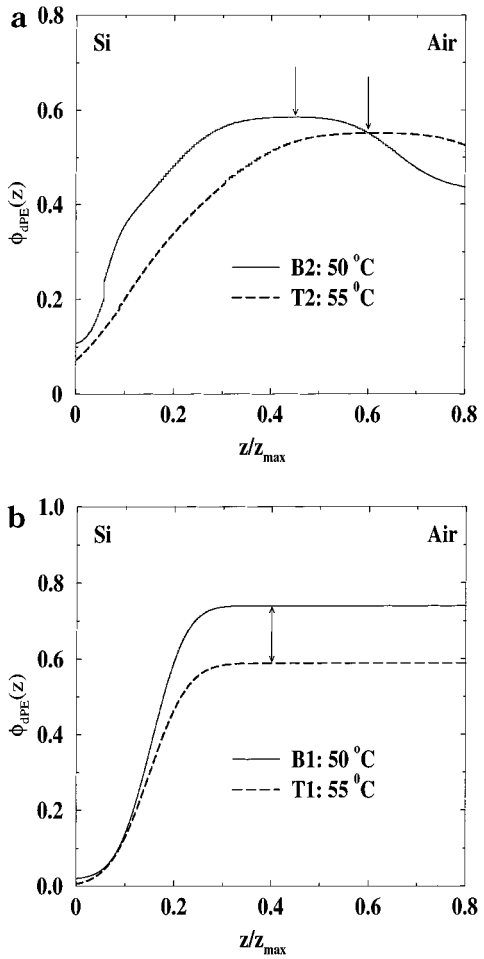

Figure 8. Concentration depth profiles for (a) molecularly thin films and (b) thin films plotted as a function of the normalized film thickness z/z_{max}, where z_{max} is the film thickness (Table 1). At these temperatures, the pinned layered structure suppresses lateral phase separation such that no changes in the profiles are observed in a 24 h period.

evaluate the effect of the attraction of hydrogenated material to silicon and air on the distribution of dPE, hPM, or hPM/hPE−hPM in the layered structure formed in the blend films.

To study the effects of film thickness and diblock copolymer on the short- and long-term stability of the blend films, optical micrographs of as-cast, "fully annealed" and long-term stored "fully annealed" films were obtained. The "fully annealed" blend films were stored under vacuum at room temperature, and optical micrographs for these films were obtained periodically over the course of a year. Typical optical micrographs of the "fully annealed" blend films are shown in Figure 9. In Figure 9a, large-scale surface features suggested by NR and XRR are observed in B1 while a dramatic suppression of these features is observed as expected for B2 (Figure 9b), T1 (Figure 9c), and T2 (Figure 9d). In view of our NR and XRR measurements, these results indicate that large-scale surface features can be suppressed by the addition of a block copolymer to a binary mixture. For the molecularly thin films, the surface enrichment of one blend component can result in stable films. After several months, a droplet morphology is still observed for B1, while one observes the development of large-scale surface features for T1 and smaller scale features for B2 and T2 (Figure 10).

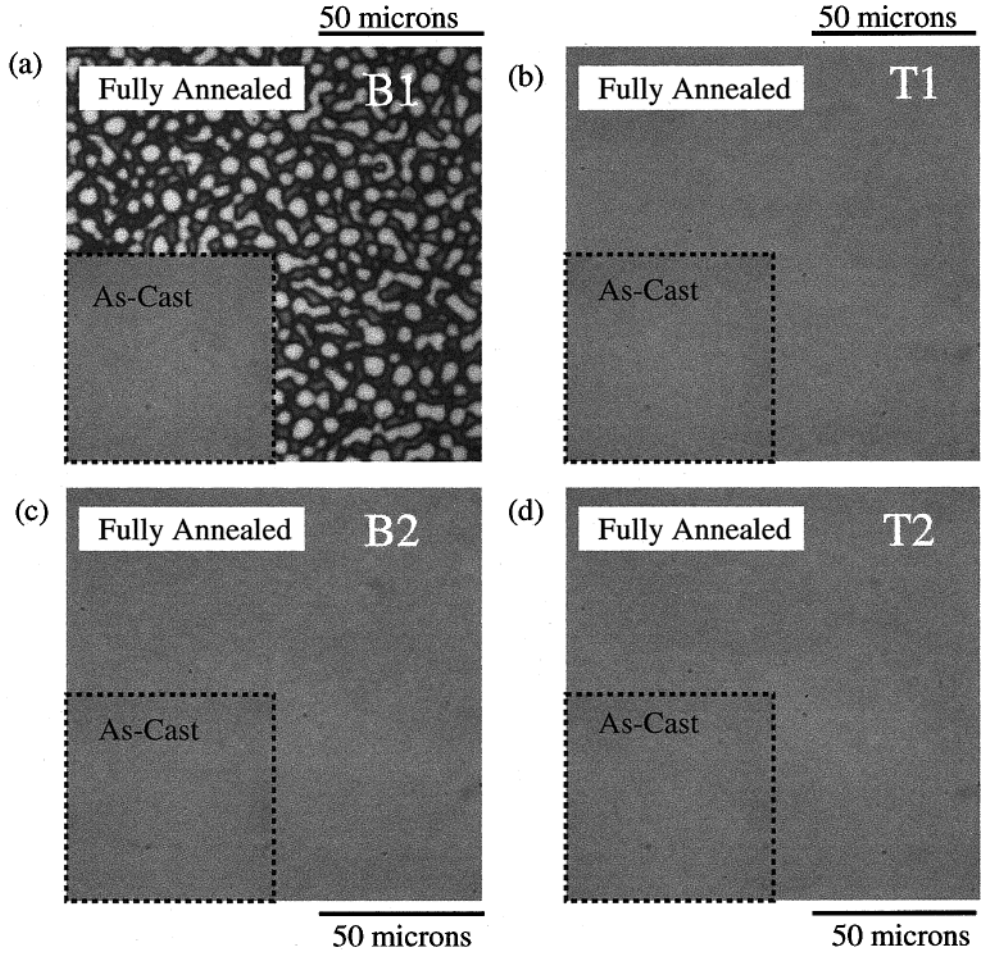

Figure 9. Optical micrographs of as-cast and "fully annealed" blend films: (a) B1, (b) T1, (c) B2, and (d) T2.

Discussion

The development of surface undulations in B1 is consistent with the surface patterns observed during lateral phase separation of near critical thin binary blend films.[22,23] Initially, as-cast films of B1 are smooth (Figure 1a) in which hPM preferentially enriches near both the air and silicon interface (Figure 2). It seems likely that the temperature (room temperature) at which the as-cast films were prepared is much lower than the critical temperature of the film leading to relatively narrow interface width, and hence a "trilayered" structure can be formed. At some higher crossover temperature (upon approaching closer to T_c), presumably due to the broadening of the hPM rich−dPE rich interfaces (presumably due to a combination of thermodynamics and capillary waves) suggested by our NR measurements, it is more favorable to phase separate within the plane of the film where there is no restriction on the interfacial width between phases. A direct consequence of lateral phase separation is the variation of surface tension within the film leading to a buckling of the film free boundary (air or vacuum) (Figure 11).[15,22] As measured by NR and XRR, the lateral phase separation process results in substantial broadening of the air−hPM rich interface, the interfaces between hPM rich and dPE rich layers, and to a lesser extent the hPM rich Si interface.[50]

There are a number of physical factors that must be considered when considering molecularly thin films. Recent Monte Carlo simulations[27] of very thin binary polymer blend films whose thickness range spans molecularly thin and thin films ($1 < D/R_g < 7$) show that the coexistence curve is shifted to smaller values of the inverse Flory−Huggins parameter χ (which is proportional to temperature) with decreasing film thickness. This observation was attributed to finite size effects alone since it occurs for "neutral" surfaces.[28] When either surface attracts the same component, which is the case in our measurements, a further lowering of the coexistence curve (an additional stabilization) is predicted from mean field simulation results.[27] The additional stabilization results from the surface enrichment of one blend component. For a given thickness, as one increases the strength of the surface interaction, the in-plane composition profile becomes more asymmetric while no additional lowering of the phase boundary is observed.

For the case where there is a preferential attraction of one component to the surface, the mean field simulation results show that the critical temperature of a symmetric binary blend is depressed by about 12% when the film thickness is about 5 times the radius of gyration.[28] The thickness of B1 is about 5 times the average radius of gyration of hPM and dPE. This means that the critical temperature in this blend should be reduced from a bulk value of 130 °C[14] to about 114 °C. This temperature (114 °C) is 15 °C higher than our highest NR temperature. Since the interfacial width varies inversely with proximity to the phase boundary (quench depth), one expects a more substantial broadening of the interface as the in-situ NR temperature is increased from room temperature to 99 °C than if the

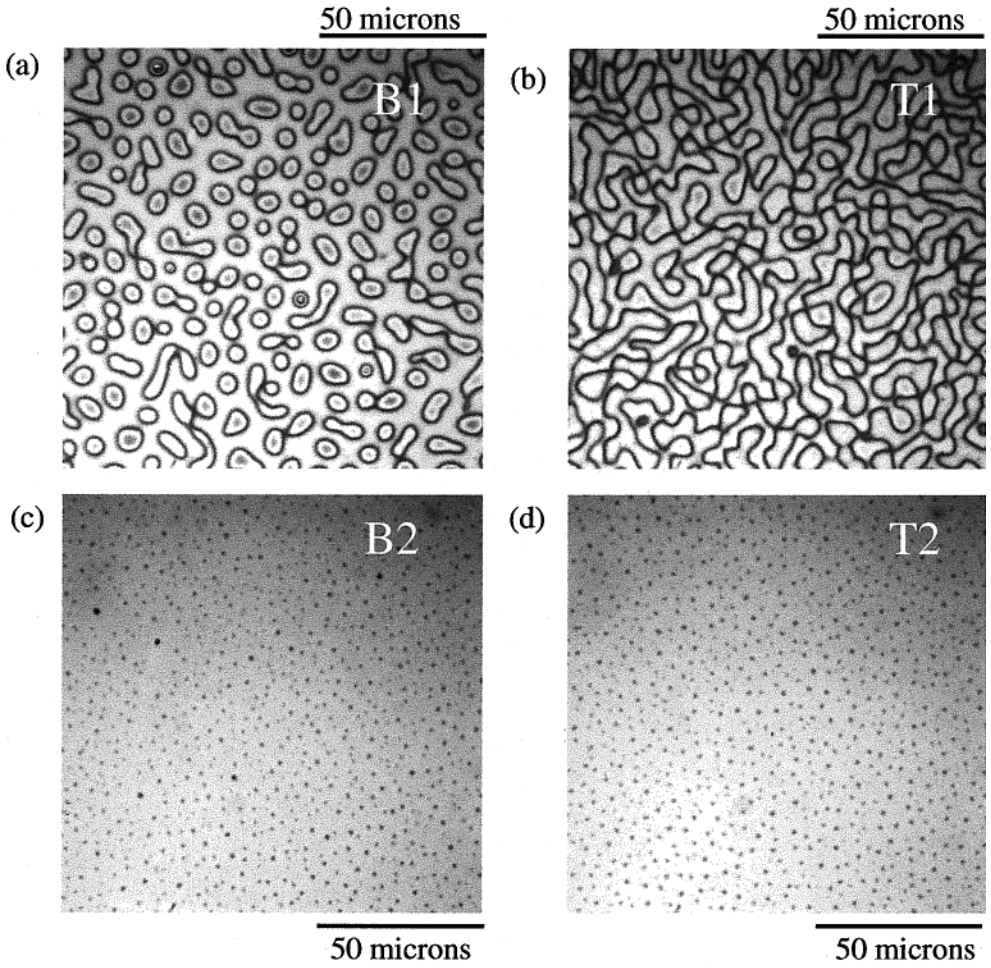

Figure 10. Optical micrographs of "fully annealed" blend films stored under vacuum for several months: (a) B1 after 7 months, (b) T1 after 7 months, (c) B2 after 12 months, and (d) B2 after 12 months.

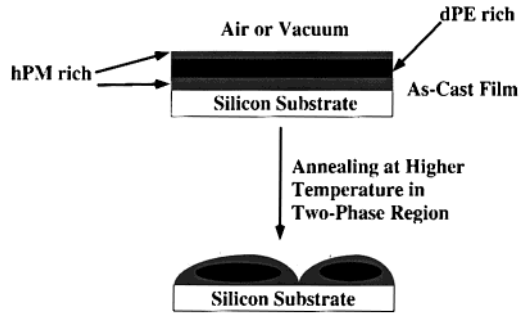

Figure 11. Schematic cross-sectional sketch showing the formation of surface patterns in dPE/hPM thin films. The top figure shows as-cast dPE/hPM films where hPM preferentially enriches both the air and silicon substrate interface. The bottom figure shows the changes resulting when thermal fluctuations resulting in lateral phase separation can overcome the pinning effect of the layered structure when the sample is further annealed in the two-phase region. A direct consequence of lateral phase separation is the variation of surface tension within the film. A manifestation of this variation is the buckling of the free boundary (air or vacuum).

critical temperature of the blend film was unchanged from 130 °C.

The stabilization of the layered structure above 74 °C in T1, can likely be attributed to a decrease in the bulk value of the UCST temperature (80 °C) in the ternary thin film. On the basis of the simulation results on binary blends, the critical temperature in T1 should be about 70 °C. This lowering is based on the preferential attraction of air and silicon for the hPM and hPM−hPE and/or finite size effects. At 74 °C, T1 maybe in the single-phase state or in a weakly quenched two-phase state. Since T1 domains ultimately evolved at room temperature, any additional lowering of the bulk critical temperature (80 °C) in the thin film results in a blend film T_c still well above 25 °C, which is consistent with the simulation predictions.

For molecularly thin films ($D \sim R_g$), a direct comparison of our results with simulation results[28] cannot be made. When the film thickness is on the order of R_g, chain configurations are distorted to an extent that the theoretical basis of the computational methods used are no longer valid. However, Monte Carlo simulations for symmetrical binary blends confined between neutral surfaces predict a 30% decrease in the critical temperature when the relative film thickness is reduced from $D/R_g = 5$ to $D/R_g = 2$ and a 38% decrease when $D/R_g = 1$. This additional lowering of the phase boundary can have a large impact on the rate of coarsening of phase-separated domains. The relative insensitivity of the b/v profiles for B2 to temperature in the range that interface broadening was observed for B1 suggests a further lowering of the critical temperature in B2. However, the blend film T_c may still be above room temperature since B2 (Figure 10c) and T2 (Figure 10d) also develop a droplet morphology with an average domain radius of about 1 μm after several months under vacuum. Our results indicate that on the time scale of the NR measurements the kinetics of phase separation in the

molecularly thin films is too slow to resolve any changes in the spectra that could be attributed to phase separation. The average radius for B2 and T2 domains are smaller than that for B1 (6 μm) and T1 (4.5 μm). The smaller droplet radius in the molecularly thin films is due to film confinement effects. Since the thickness of the molecularly thin films is on the order of R_g, large length scales of lateral phase separation are not sustained in these films. It is interesting to note that the average domain radius of 6 μm obtained for B1 immediately after annealing is unchanged after several months. In T1, the addition of block copolymer slows down the coarsening of domains even further such that an interconnected morphology characteristic of the early to intermediate stages of phase separation persists after 6 months (Figure 10b).

For the blends studied in the present paper, the addition of a diblock copolymer (hPM−hPE) to a binary mixture of hPM and dPE has been shown to increase the phase stability of bulk films.[14] Rice and Cahn have shown that any third component that lowers the phase transition temperature (increases the phase stability) of a binary mixture must, at equilibrium, be present in excess at the interface between coexisting phases.[51,52]

On the basis of these works, one expects interfacial segregation of block copolymer in any phase-separated mixture of two homopolymers and a block copolymer. As mentioned previously, the asymmetry in the b/v profiles in the molecularly thin blend films (Figures 6 and 7) can be attributed to the strong attraction of hydrogenated species (hPM and/or hPE) to the passified silicon surface compared to the attraction of these materials to the air interphase. Figure 8 shows the concentration depth profiles for the blend films studied. The concentration at $z/z_{max} > 0.8$ is not shown since the film/air roughness is convoluted into the composition profile in an undetermined way. In the molecularly thin films, the stronger attraction for hydrogenated material results in a higher concentration near the Si interface when hPE−hPM is a blend component (Figure 8a). Thus, the pronounced rounding of the polymer−polymer interface (compare parts a and b of Figure 8) observed near the silicon boundary can be due to the lowering of the surface tension by the diblock copolymer (Figure 8). In the highest scattering length phase near $z/z_{max} = 0.45$ for B2 and $z/z_{max} = 0.6$ for T2, there is a small reduction of the concentration of dPE (see arrows in Figure 8a). The concentrations of dPE are 0.59 for B2 and 0.55 for T2 (Figure 8a). Since these difference are minor, i.e., comparable to the average deviation (3%) in the b/v values used to estimate $\phi_{dPE}(z)$, most of the protonated diblock must be mainly located at the polymer interphase near the Si boundary in molecularly thin films. It is interesting to note that the asymmetric composition−depth profiles predicted from mean field simulations[28] of the phase separation of thin polymer blend films near strongly attractive surfaces is observed for molecularly thin films.

In the thin films, the asymmetry in the shape of the b/v profiles and hence in the composition−depth profiles is less pronounced, suggesting that the range of the surface interaction is much smaller than the thickness of the film. However, in the highest scattering length density phase near $z/z_{max} = 0.5$, there is a significant reduction of the concentration of dPE in the presence of diblock (see double arrow in Figure 8b); i.e., $\phi_{dPE}(z)$ is 0.74 for B1 and 0.59 for T1 (Figure 8b). This large reduction coupled with the higher concentration of hydrogeneous material at both the silicon and air interphase indicates that diblock is distributed throughout the film. This conclusion is also consistent with the conclusion drawn from the previous bulk phase separation studies by Balsara et al.[14] In these bulk film studies, experimental evidence indicates that there is a uniform distribution of diblock throughout the sample during all stages of phase separation. We hope that the good agreement between our results for the binary blend and previous simulations will stimulate further simulation work on ternary systems which addresses the issue raised and the generality of the results of this paper.

Conclusions

The effectiveness of a compatibilizer in suppressing lateral phase separation in thin films is investigated as a function of film thickness and temperature. For molecularly thin films (≈25 nm), finite size effects and the surface enrichment of the hydrogenated blend components (hPM in the binary blends and hPM/hPE−hPM in ternary blends) stabilize the layered structure. For thin films (≈100 nm), the development of large-scale phase separation-induced surface roughness is suppressed when the block copolymer compatibilizer is a blend component. We attribute this stabilization effect to the reduction of interfacial tension and presence of diblock copolymer in both phases and at the interfaces. After several months, the molecularly thin blend films develop a droplet morphology with an average domain size of 1 μm while an interconnected domain structure with an average domain size of 4.5 μm is observed for the ternary thin blend film. The phase-separated structure obtained for the binary thin blend film does not evolve at room temperature as the size the domain size (6 μm) is unchanged after several months. Since domains for the blend films studied evolved at room temperature, the expected lowering of the phase boundary from finite size effects and the compatibilization of the block copolymer must result in a critical temperature still well above room temperature. Our studies show that one also needs to account for kinetics in order to develop a comprehensive understanding of the structure of thin blend films. In effect, polymer blend films are slowly evolving metastable states.

Acknowledgment. We thank Dr. Holger Gruell and Dr. Robert Ivkov at the NIST for their assistance during the Neutron Reflectivity experiments and for their discussions. We thank Dr. Jack Douglas for his many helpful suggestions and discussions and for suggesting the term molecularly thin films.

References and Notes

(1) Russell, T. P. *Mater. Sci. Rep.* **1990**, *5*, 171.
(2) Wu, S. *Polymer Interfaces and Adhesion*; Marcel Dekker: New York, 1982.
(3) Vrij, A. *Discuss. Faraday Soc.* **1966**, *42*, 23.
(4) Vrij, A.; Overbeek, J. T. G. *J. Am. Chem. Soc.* **1968**, *90*, 3074.
(5) Brochard, F.; Dalliant, J. *Can. J. Phys.* **1990**, *68*, 1084.
(6) Milchev, A.; Binder, K.; Vrij, A. *J. Chem. Phys.* **1997**, *106*, 1978.
(7) Reiter, G. *Macromolecules* **1993**, *27*, 3046.
(8) Reiter, G. *Langmuir* **1993**, *9*, 1344.
(9) Reiter, G. *Phys. Rev. Lett.* **1992**, *68*, 75.
(10) Stange, T. G.; Evans, D. F.; Hendrickson, W. A. *Langmuir* **1997**, *13*, 4459.
(11) Xie, R.; Karim, A.; Douglas, J. F.; Han, C. C.; Weiss, R. A. *Phys. Rev. Lett.* **1998**, *81*, 1251.

(12) Hashimoto, T. In *Materials Science and Technology*; Thomas, E. L., Ed.; VCH: Weinheim, 1993; Vol. 12, p 251.
(13) Balsara, N. P.; Jonnalagadda, S. V.; Lin, C. C.; Han, C. C.; Krishnamoorti, R. *J. Chem. Phys.* **1993**, *99*, 10011−10020.
(14) Lin, C. C.; Jeon, H. S.; Balsara, N. P.; Hammouda, B. *J. Chem. Phys.* **1995**, *103*, 1957−1971.
(15) Sung, L.; Nakatani, A. I.; Han, C. C.; Karim, A.; Douglas, J. F.; Satija, S. K. *Physica B* **1998**, *241*−*243*, 1013−1015.
(16) Jones, R. A. L.; Norton, L. J.; Kramer, E. J.; Bates, F. S.; Wiltzius, P. *Phys. Rev. Lett.* **1991**, *66*, 1326.
(17) Bruder, F.; Brenn, R. *Phys. Rev. Lett.* **1992**, *69*, 624.
(18) Krausch, G.; Dai, C.-A.; Kramer, E. J.; Bates, F. S. *Phys. Rev. Lett.* **1993**, *71*, 3669.
(19) Krausch, G.; Dai, C.-A.; Kramer, E. J.; Marko, J. F.; Bates, F. S. *Phys. Rev. Lett.* **1993**, *26*, 5566.
(20) Krausch, G.; Kramer, E. J.; Rafailovich, M. H.; Sokolov, J. *Appl. Phys. Lett.* **1994**, *64*, 2665.
(21) Sung, L.; Karim, A.; Han, C. C. *Phys. Rev. Lett.* **1996**, *76*, 4368−4371.
(22) Ermi, B. D.; Karim, A.; Douglas, J. F. *J. Polym. Sci., Polym. Phys.* **1998**, *36*, 191.
(23) Karim, A.; Slawecki, T. M.; Kumar, S. K.; Douglas, J. F.; Satija, S. K.; Han, C. C.; Russell, T. P.; Liu, Y.; Overney, R.; Sokolov, J.; Rafailovich, M. H. *Macromolecules* **1998**, *31*, 857−862.
(24) Genzer, J.; Kramer, E. J. *Phys. Rev. Lett.* **1997**, *78*, 4946.
(25) Marko, J. F. *Phys. Rev. E* **1993**, *48*, 2861.
(26) Jandt, K.; Heier, J.; Bates, F. S.; Kramer, E. J. *Langmuir* **1996**, *12*, 3716.
(27) Rouault, Y.; Baschnagel, J.; Binder, K. *J. Stat. Phys.* **1995**, *80*, 1009.
(28) Flebbe, T.; Dunweg, B.; Binder, K. *J. Phys. II* **1996**, *6*, 667−695.
(29) Bates, F. S.; Maurer, W. W.; Lipic, P. M.; Hillmyer, M. A.; Almdal, K.; Mortensen, K.; Fredrickson, G. H.; Lodge, T. P. *Phys. Rev. Lett.* **1997**, *79*, 849−852.
(30) Fredrickson, G. H.; Bates, F. S. *J. Polym. Sci., Part B: Polym. Phys.* **1997**, *35*, 2775−2786.
(31) Mortensen, K.; Almdal, K.; Schwahn, D.; Bates, F. S. *J. Appl. Crystallogr.* **1997**, *30*, 702−707.
(32) Kielhorn, L.; Muthukumar, M. *J. Chem. Phys.* **1997**, *107*, 5588−5608.
(33) Koneripalli, N.; Levicky, R.; Bates, F. S.; Matsen, M. W.; Satija, S. K.; Ankner, J.; Kaiser, H. *Macromolecules* **1998**, *31*, 3498−3508.
(34) Kielhorn, L.; Muthukumar, M. *J. Chem. Phys.* **1999**, *110*, 4079−4089.
(35) Lyatskaya, Y.; Jacobson, S. H.; Balazs, A. C. *Macromolecules* **1996**, *29*, 1059−1061.
(36) Gersappe, D.; Irvine, D.; Balazs, A. C.; Liu, Y.; Sokolov, J.; Rafailovich, M.; Schwarz, S.; Peiffer, D. G. *Science* **1994**, *265*, 1072−1074.
(37) Dudowicz, J.; Freed, K. F.; Douglas, J. F. *Macromolecules* **1995**, *28*, 2276.
(38) Israels, R.; Jasnow, D.; Balazs, A. C.; Guo, L.; Krausch, G.; Sokolov, J.; Rafailovich, M. *J. Chem. Phys.* **1995**, *102*, 8149−8157.
(39) Lyatskaya, Y.; Gersappe, D.; Balazs, A. C. *Macromolecules* **1995**, *28*, 6278−6283.
(40) Lyatskaya, Y.; Balazs, A. C. *Macromolecules* **1996**, *29*, 7581−7587.
(41) Lyatskaya, Y.; Gersappe, D.; Gross, N. A.; Balazs, A. C. *J. Phys. Chem.* **1996**, *100*, 1449−1458.
(42) Guo, H. F.; Packirisamy, S.; Gvozdic, N. V.; Meier, D. J. *Polymer* **1997**, *38*, 785−794.
(43) Zhu, S.; Liu, Y.; Raifailovich, M. H.; Sokolov, J.; Gersappe, D.; Winesett, D. A.; Ade, H. *Nature* **1999**, *400*, 6739.
(44) Sung, L.; Karim, A.; Douglas, J. F.; Han, C. C. *Polym. Prepr., Am. Chem. Soc. Div. PSME* **1996**, *74*, 106−107.
(45) Higashi, G. S.; Chabal, Y. J.; Trucks, G. W.; Raghavachari, K. *Appl. Phys. Lett.* **1990**, *56*, 656−658.
(46) According to ISO 31-8, the term molecular weight has been replaced by "relative molecular mass" M_r. Thus, if this nomenclature and notation were to be followed in this publication, one would write $M_{r,n}$ instead of the historically conventional M_n for the number-average molecular weight, with similar changes for M_w, and it would be called the "number-average relative molecular mass." The older more conventional notation, rather than the ISO notation, has been employed for this publication.
(47) Certain equipment and instruments or materials are identified in the paper in order to adequately specify the experimental details. Such identification does not imply recommendation by the National Institute of Standards and Technology, nor does it imply the materials are necessarily the best available for the purpose.
(48) Anker, J. F.; Majkrzak, C. F. *SPIE: Neutron Optical Devices and Applications* **1990**, *1738*, 260.
(49) Parratt, L. G. *Phys. Rev.* **1954**, *95*, 359.
(50) The complete dissolution of the phase-separated structure in B1 is not observed even when the sample is annealed above the bulk phase separation temperature for several hours. We believe from past measurement experience[22] that the homogenization by annealing in the single phase is possible only when the phase separation has not proceeded to late stages.
(51) Rice, O. K. *J. Chem. Phys.* **1976**, *64*, 4362.
(52) Cahn, J. W. In *Interfacial Segregation*; Johnson, W. C., Blakey, J. M., Eds.; ASM: Metals Park, OH, 1979; p 3.

MA001347P